DEVELOPMENT OF A COMPENSATED INTERFEROMETRIC DETECTOR

By

Braden Michael Durbin

Thesis

Submitted to the Faculty of the

Graduate School of Vanderbilt University

in partial fulfillment of the requirements

for the degree of Chemistry

MASTER OF SCIENCE

in

CHEMISTRY

May, 2015

Nashville, Tennessee

Approved:

Darryl J. Bornhop, Ph.D.

Carmelo J. Rizzo, Ph.D.

ACKNOWLEDGMENTS

Throughout my time in graduate school I have several people to thank. First, I would like to thank my advisor, Dr. Darryl Bornhop. I would like to thank him for the time, support, and encouragement that he provided during my studies. I would not have been able to complete this degree without him, and much of my growth as a scientist is because of him. Next, I would like to thank all of the members of the Bornhop lab especially Amanda, Lynn, Michael, Tim, Kaitong, and Nancy. Being able to work with such great people made working much more enjoyable.

I also want to thank my family for their love and support. I want to thank them for instilling in me a love of learning and fostering an interest in science at an early age. I also would like to thank my family for encouraging me in the difficult times, and the busy times.

I also would like to thank my friends outside of the lab at Vanderbilt for their support and encouragement. They have made my time at Vanderbilt very enjoyable, and I am very thankful to call them my friends.

Lastly, I would like to thank Vanderbilt University for providing me an opportunity to continue my education and for their financial support, specifically the Department of Chemistry, the Arthur William Ingersoll Memorial funds, and a Vanderbilt Discovery Grant which funded the work presented in this thesis.

TABLE OF CONTENTS

LIST OF TABLES

LIST OF FIGURES

LIST OF ABBREVIATIONS

BioCD biological compact disk

BLI Biolayer Interferometry

BSI Backscattering Interferometry

CCD Charge-coupled device

DCDB dual capillary backscattering interferometry

DPI dual polarization interferometry

FEP fluorinated ethylene propylene

FFT fast Fourier transform

hCG human chorionic gonadotropin

LOQ limit of quantification

NMR nuclear magnetic resonance

PBS phosphate buffered saline

PDMS polydimethylsiloxane

PSA prostate-specific antigen

RI refractive index

RIU Refractive Index Unit

SPR surface plasmon resonance

CHAPTER I

Introduction

A wide variety of assays and platforms have been developed over the years to aid in answering a single question: how do two molecules interact with one another? This simple question has a huge impact on our lives. Interaction assays are used in the detection of biomarkers which indicate the possible presence of a disease such as cancer. Interaction assays are also used to a) detect pollutants which could harm our bodies or the environment and b) determine the mechanisms of actions between molecular or ionic binding pairs. Interaction assays play a major role in the pharmaceutical industry, using them to determine the performance of potential new drugs based on their affinity for a specific target as well as to determine the drug doses that should be administered when undergoing clinical trials.

A variety of platforms have been used to study molecular interactions, including UV-vis, fluorescence, NMR and mass spectrometry. While these techniques have their benefits, they also have drawbacks and limitations. For instance, UV-vis or fluorescence can only be performed on molecule which absorbance or fluorescence. In the absence of native fluorescence, a label must be added to one or both of the interacting species possibly impacting the behavior of the molecule of interest and increasing the complexity of the assay. Labels can interfere with the binding between two partners by inducing steric hindrance or also by blocking the binding site. These factors could greatly lower the interactions of two suspected binding partners. By where the label is placed on a species, the observed interaction could be vastly different than if the label is placed somewhere else on the species. There are also a great number of difficulties in labelling. If there is a high variability in the labelling efficiency, it would be hard to determine the binding energy or expression level with any real confidence. Commonly, a label is used which is fluorescent. The fluorescence signal can be impacted by a variety of environmental factors such as temperature, pH, and

local field intensity. Fluorescent labels are also subject to quenching and bleaching. A false fluorescent signal can also be observed if there is nonspecific background binding causing the labels to fluoresce, as well as autofluorescence of compounds in the matrix that is being analyzed (*1*, *2*). To fully understand how molecules interact, these interactions should be interrogated without the use of labels. To address this need, numerous label-free techniques have been developed to measure chemical interactions. These devices typically measure the universal property of refractive index (RI).

Interestingly, the RI of a fluid can be used to measure molecules binding to one another without the need for labels. It has been shown that factors such as a molecules conformation, charge distribution, and hydration all effect the RI of the fluid that they are contained in. It has also been shown that RI can be impacted by molecular structure, dipole moment, and polarizability (*3*–*5*).

I.1 Refractive Index

RI is a measure how light propagates through a medium. Specifically, the RI (n) of a given medium is the ratio of the speed of light (c) in a vacuum compared to the speed of light in that given medium (v) (Equation I.1). Water has an RI of $n = 1.33219$ which means that light travels through water at a speed that is approximately 25% less than the speed of light in a vacuum which has been given an index of refraction of $n = 1$. When entering from one medium to another of a different RI, light is bent or refracted at an angle. The angle and how the light will propagate when passing through the interface are defined by Snell's Law (Equation I.2). That the ratio of the sines of the angle of incidence, θ_i, and angle of refraction, θ_r of incoming light are equal to the ratio of the RI of medium through which the light is refracted, n_r and the RI of the medium through which incident light travels, n_i.

$$n = \frac{c}{v} \tag{I.1}$$

The approaches existing to quantify the RI of a material, range from simple deflection to interferometry. Most non-interferometric approaches capitalize on the fact that when traversing from one medium to another of a different RI, light will be bent or refracted at an angle. The angle and how the light will propagate when passing through the interface are defined by Snell's Law (Equation I.2). That the ratio of the sines of the angle of incidence, θ_i, and angle of refraction, θ_r of incoming light are equal to the ratio of the RI of medium through which the light is refracted, n_r and the RI of the medium through which incident light travels, n_i.

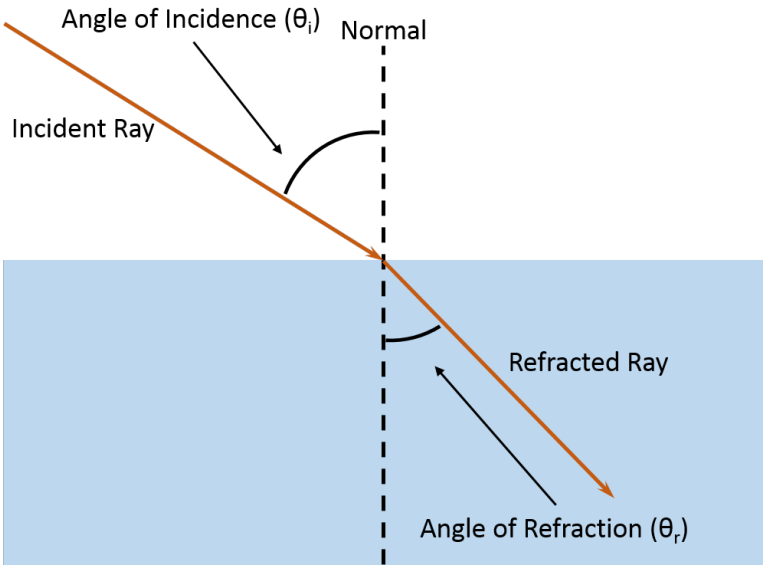

Figure I.1: Refraction of a ray of light

$$\frac{\sin\theta_r}{\sin\theta_i} = \frac{n_i}{n_r} \tag{I.2}$$

I.1.1 Environmental Factors that Impact Refractive Index

The RI of a medium is impacted by several physical properties. The major factors are the temperature and the pressure of the sample, and the wavelength of light being used. Both temperature and pressure have a huge impact on the matrix RI, which is important when attempting to measure molecular interactions by detecting binding induced molecular

dipole changes. To function in most biochemical assays, a RI sensor must be able to detect a change of RI on the order of 10^{-5} RIU or lower (*6*). For water, at a wavelength of 632.8 nm, the $\frac{dn}{dT}$ sensitivity is on the order of $1x10^{-4}$ RIU per degree Celsius in the range of 20-30°C (*7*). Therefore, to perform an assay with an RI sensor the temperature must be controlled to within a millidegree.

One approach used to mitigate temperature-induced noise is to control the detection zone actively with a Peltier or passively with a large thermal mass. In either case the sample must come to equilibrium prior to making subsequent determinations. In this regard, microfluidic chips serve as excellent sample holders because of their large thermal mass which surrounds the sample fluid. Other common approaches is to measure both sample and reference simultaneously (*6*, *8–13*).

Pressure does not affect RI to the extent that temperature does, but it is significant. At a temperature of 24.5°C, the change of RI based on changes in pressure, $\frac{dn}{dbar}$, is approximately $1x10^{-5}$ RIU. Therefore to make measurements at the desirable level of ca. 10^{-6}–10^{-7} ΔRI, the run-to-run pressure stability must be controlled to within 10 mbar.

I.1.2 Differential Refractometry

Differential refractometry is one of the most common approaches used to measure RI of a solution. Differential measurements can take several forms, including, deflection, interferometric, and Fresnel reflection (*14*). One widely used instrument features a square flow cell which is divided diagonally, separating a sample region and a reference region. As shown in the diagram (Figure I.2), monochromatic light passes through both regions of the flow cell, the refracted rays are then collected by a collimating lens which directs the rays onto the bicell photodetector. The device measures the relative RI of the reference and sample regions of the flow cell. If they are identical, have zero difference in RI, the incident rays of light will be *equally* refracted and will emerge parallel to the incident radiation. Centering the detector on this spot, equally illuminating each side of the photodiode serves

as the baseline, or the zero position. With proper alignment and the same fluid RI in the cells, the difference in current between the two photodiodes will be zero. When the RI of the sample inside of the cell changes, incident rays will be refracted causing a shift in the position of outgoing light impinges on the detector. Since the position of the light impinged on the detector has now changed, one photodiode is now receiving more light than the other resulting in a difference in current which is non zero. By monitoring the changes in current, the change in position of the refracted light can be determined and the angle of refraction can be calculated. Knowing the RI of the reference and the angle of the incident light, the unknown index of refraction can be calculated.

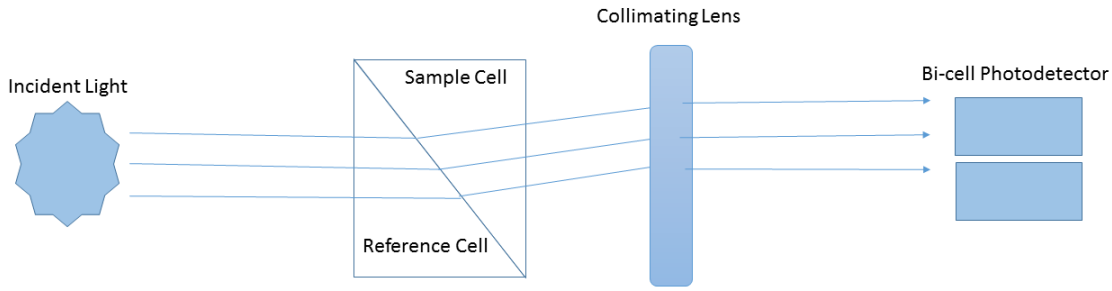

Figure I.2: Diagram of a differential refractometer

The instrument is capable of compensating for changes in temperature because the measurement is differential in nature. Both sample and reference fluids are measured simultaneously. If the temperature of each fluid changes by the same amount, the RI of both sample and reference will also change the same amount, but the difference in RI between the sample and reference will not be affected. However, this detector is most commonly used in HPLC systems which requires the use of active temperature control in order to min-

imize thermal gradients in a flow cell and to avoid thermal differences between the sample and reference fluids (*15*).

I.2 Interferometry

Interferometry accurately measures the RI, by determining the change in the speed of light for waves that have been made to interact with one another. As shown by Thomas Young's double slit experiment (Figure I.3), when monochromatic light is passed through two closely spaced slits the light interacts producing a series of bright fringes caused by interference between the two sets of waves originating from each slit.

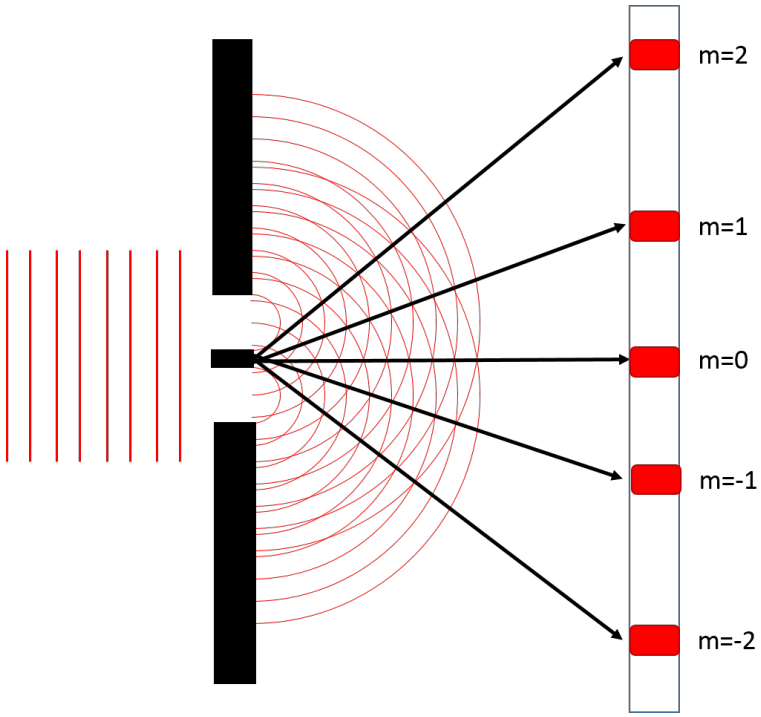

Figure I.3: Thomas Young's double slit experiment.

Waves are sinusoidal functions, so if two sinusoidal functions have the same frequency, amplitude, and are in phase, constructive interference occurs. The resulting function will have the same frequency as the two separate functions, but the amplitude will be two times greater than the amplitude of one of the original functions (Figure I.4a). If the two functions are exactly out of phase, the interference between the two waves will produce a resultant

function that can be both constructive and destructive. When the two waves are 180° different in phase, the resulting function will be a flat line with no amplitude (Figure I.4b). This is the most extreme example of destructive interference.

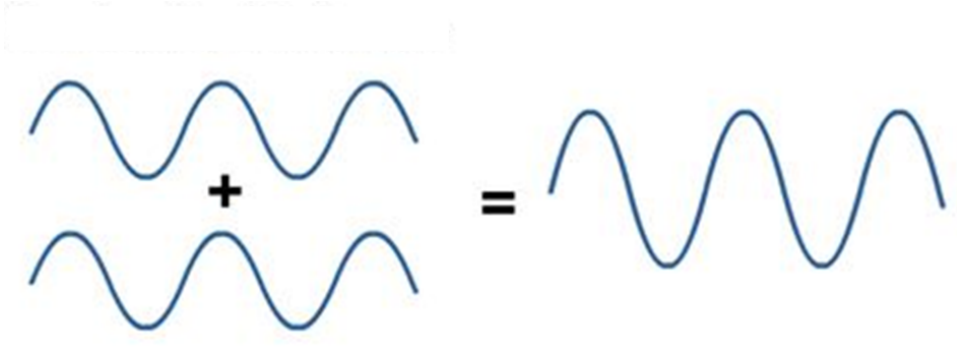

(a) Constructive Interference

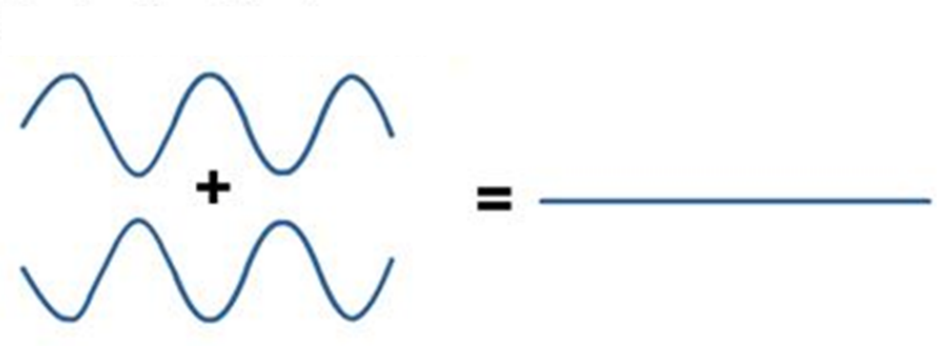

(b) Destructive Interference

Figure I.4: Interference of sinusoidal waves.

Over the years, interferometry has been the basis for a number of instruments that have been developed for a wide variety of uses spanning many fields such as astronomy, metrology, seismology, and biological sciences (*16–22*). Interferometry was first used on the cosmic level over two centuries ago to discover why stars appear larger through a telescope in comparison to other objects. It has also been used to determine the actual sizes of objects in our solar system and beyond. Interferometry has also been useful on a much smaller scale as a method to quantify the level of interaction between molecules, including those which are biologically relevant.

Interferometers are extremely useful in characterizing molecular interactions because they do not require the use of chemical labels such as methods like luminescence. By adding a label to one or both binding partners, the system has been inherently changed and could easily lead to observing a binding affinity which is significantly different than the actual binding affinity.

I.2.1 Mach-Zehnder Interferometer

The Mach-Zehnder interferometer is an evanescent-field refractive interferometer in which light from a laser is split and guided through a separate sample and reference region and then recombined before being detected (Figure I.5). Specifically, light from a laser illuminates a single-mode waveguide which is then split into a sample and reference arm. The reference arm is coated with a thin cladding while the sample arm contains a window through which the evanescent field can interact with the sample. If there is any change in the RI of the sample arm, such as can be caused by the binding of two different species, the phase of the light in the sample arm will shift. The reference and sample beams are then recombined causing interference between the light that passed through the separate arms. The difference in RI is then correlated to the relative change in intensity of the laser light detected by a photodiode detector (*23*).

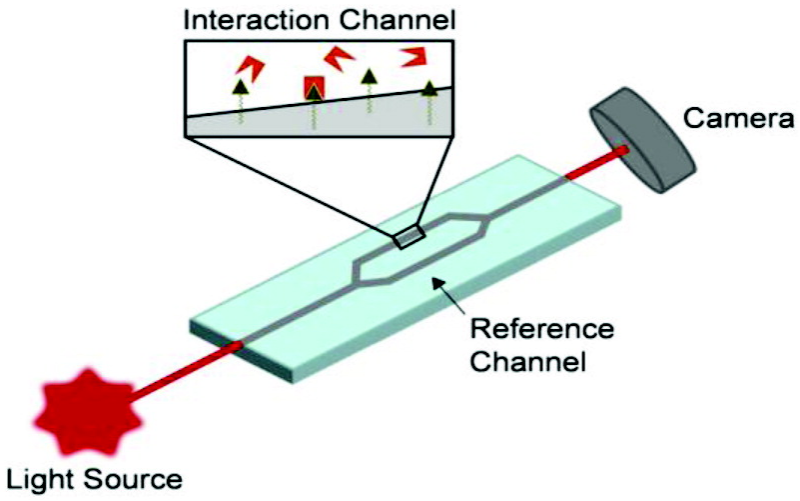

Figure I.5: Diagram of a Mach-Zehnder Interferometer (*23*).

This method has been able to detect RI changes as small as $7x10^{-6}$ RIU (*6*). The sensitivity of the device is dependent upon the length of the sample window. A longer window increases the sensitivity of the device. A hindrance to having a longer window is that it can also require that a larger sample volume must be used (*8*). One of the biggest advantages of this device is its ability to effectively compensate for temperature induced drift (*9*). Initial experiments demonstrative experiments showed nonspecific binding of fetal calf serum binding to the surface of the sensor (*6*). The instrument has also been developed into a multiplexing array while achieving sensitivity that compares well to commercial SPR by using thin silicon oxide waveguides (*9*).

I.2.2 Young Interferometer

The Young interferometer is very similar to the Mach-Zehnder interferometer. Both devices contain a single mode waveguide that splits into a sample and reference arm. The difference for the Young interferometer is that the two different arms do not recombine into a single waveguide (Figure I.6). The interference takes place as light from both waveguides interact in the open. The interference fringes that are produced are then captured by a CCD camera for analysis (*23*).

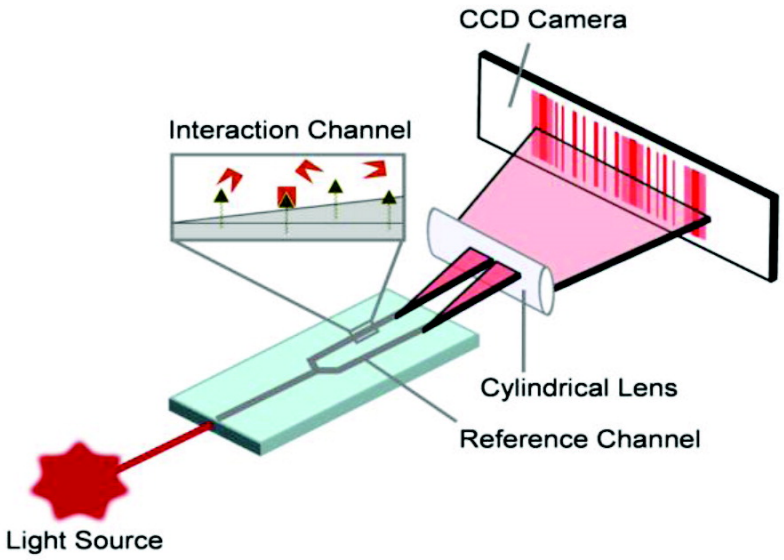

Figure I.6: Diagram of a Young Interferometer (*23*).

A major advantage of the Young interferometer is that it has been able to be multiplexed allowing for multiple analyte concentrations to be analyzed simultaneously. The multiplexing arrangement has achieved a sensitivity of $8.5 \text{x} 10^{-8}$ RIU (*10*).

I.2.3 Hartman Interferometer

The Hartman interferometer is also a waveguiding device, but it is much different than both the Mach-Zehnder interferometer, and the Young interferometer. The Hartman interferometer is a planar waveguide which is patterned with lines of immobilized molecules (Figure I.7). First, light is directed onto the waveguide by the use of a diffraction grating. The diffraction grating is used to create a single broad beam of light which passes through the sensing regions in parallel. The sensing regions are coated with different receptors to create different binding and control regions. The light then passes through optics that combine light from adjacent regions. The resulting interference pattern passes through a second diffraction grating and to a detector. To detect changes in refractive index, the phase shift of the interference patterns is measured (*23*).

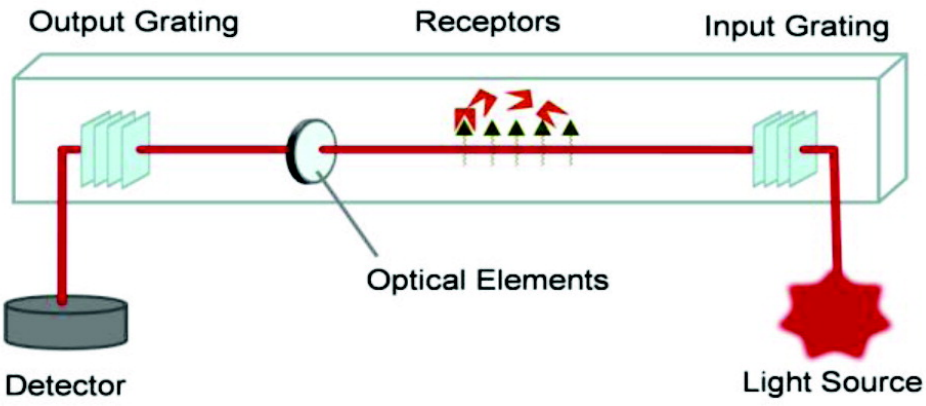

Figure I.7: Diagram of a Hartman Interferometer (*23*)

The broad applications of the Hartman interferometer have been demonstrated to a great extent including the ability to detect and measure human chorionic gonadotropin (hCG), a hormone that is produced by some cancerous tumors, in whole blood (*24*). In these experiments, the receptor, anti-hCG antibody was immobilized to the surface of the sensor.

A clinically relevant detection limit of hCG was achieved which is tremendous for a label-free sensor since whole blood has a much higher level of background noise when compared to serum and buffer systems.

I.2.4 Diffraction Optics

Diffraction optics are very similar to the Hartman interferometer. Instead of using a diffraction grating, probe molecules are immobilized onto a substrate into a pattern which will diffract incoming light to form an interference pattern. The interference pattern changes when sample is introduced and binding occurs. The changes of the interference pattern are due to changes in the height of the diffraction grating and changes in refractive index. The intensity of the refractive spots is measured using a photodetector, which allows for any changes within the sample to be measured (*23*).

One of the biggest advantages to using a diffraction based sensor is that the diffraction signal is only created when biomolecules specifically bind to a probe molecule on the patterned substrate. Nonspecific binding to the surface of the sensor does not cause a change in signal.

The device also has a good potential to be used in diagnostic applications. The technology was used to detect binding of two interactions simultaneously without use of a label. This was done by immobilizing the receptor proteins into two different patterns on the PDMS substrate. The two proteins of interest were then introduced sequentially and the binding observed for each pattern indicated the binding of the protein to its specific receptor (*25*). This technology can also be used in diagnostics using multiple biomarkers and competition assays (*26*, *27*).

The technology has been incorporated into a commercial system called the dotLab system by Axela Biosensors, which allows for the multiplexing of immunoassays over a wide dynamic range.

I.2.5 Dual Polarization Interferometry

Dual polarization interferometry is another waveguide technique used to study molecular interactions (Figure I.8). Two waveguides are stacked together so they may be illuminated by a single laser. One waveguide acts as a sample waveguide while the other acts as a reference waveguide. In this method the polarization of the laser is alternated so that two polarization modes of the waveguides are excited in succession in order to modulate the signal and increase the sensitivity of the measurement. The thickness of the adsorbed protein layer can be calculated using information such as the polarization states and RI(*23*).

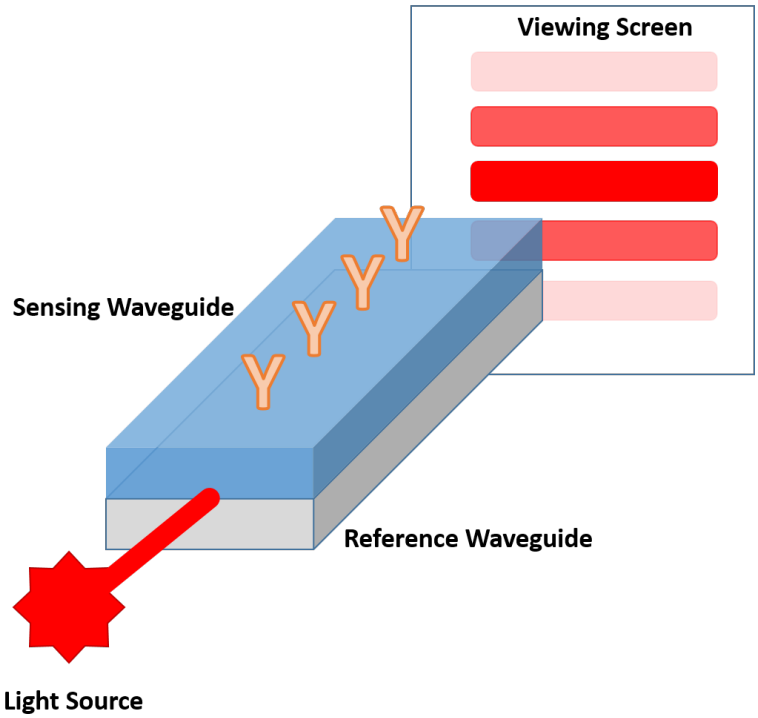

Figure I.8: Diagram of Dual polarization interferometer.

DPI has shown that it can measure a wide array of binding interactions over a large molecular range and is able to measure structure and kinetics simultaneously (*11*, *12*). Recently, the technology has been commercialized and the latest development, the AnaLight 4D, has enabled the structural change measurements inside of lipid bilayers (*28*).

I.2.6 Waveguide Microresonators

Waveguide microresonators use a circular configuration to achieve total internal reflection which increases the lifetime of a photon in the ring. For most other traditional waveguide methods, light only makes a single pass, allowing a photon to interact only once with an analyte of interest. A microresonator allows for a photon to have multiple interactions with an analyte which has been adsorbed to the surface of the microresonator. Resonance is achieved at a particular wavelength depending upon the geometry of the resonator. Resonance is disrupted when changes in the optical path length occur. Changes in the optical path length are due to changes in RI caused by molecules of interest binding to the surface of the waveguide. The greater number of passes a photon is able to circle around the microresonator leads to a higher Q factor for the device enabling greater sensitivity (*8*, *29–31*).

I.2.7 Surface Plasmon Resonance Interferometry

Many approaches have been used to capitalize on surface plasmon resonance (SPR), with the Kortzman optical train being commercialized and widely used in biosensing applications. SPR is not an interferometric method, is based on detecting surface plasmons resulting from evanescent wave sample coupling when an electromagnetic beam strikes a metal-dielectric surface. The result is electrons at the surface of the metal are excited and oscillate. SPR monitors changes in RI at the sensor surface due to the relative coupling efficiency of the light, with the resonant frequency being dependent upon the RI at the sensor surface. One of the molecules in the binding pair will be immobilized on the surface of the sensor. The other molecule of the binding pair is introduced free in solution. When binding occurs, there is a change in the RI at the surface of the sensor. At the frequency that incident light and the surface plasmon are coupled, a resonance reflectance dip is observed. Changes in the intensity of the reflected light are monitored allowing for binding to be monitored. This method has its drawbacks in that it is difficult for the device to

monitor interactions between molecules with low molecular weights. SPR interferometry was developed to gain more sensitivity than traditional surface plasmon resonance (*23*). In SPR interferometry, the phase of the reflected light is monitored instead of the intensity as done in traditional measurements. Monitoring the phase gave higher sensitivity and a wide dynamic range (*32*, *33*).

I.2.8 Porous Si, Al, Ti Sensors

Porous sensors are developed on the principles of the Fabry-Perot interferometer within substrates etched in thin films of silicon, aluminum, or titanium. Fabry-Perot interferometers rely on interference between light which reflects off of different surfaces within the sensor. In general, the porous film acts as an interferometer by light reflected off of the top and bottom of the pores interfering with one another producing an interference pattern. For applications in biology, the two surfaces may be the top and bottom interface of the sensing layer.

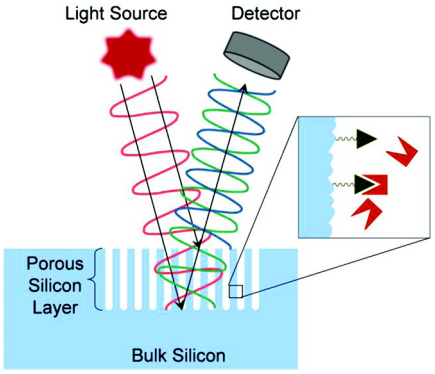

Figure I.9: Diagram of a Pourous sensor (*23*).

This type of sensor measures the optical density, which is a product of RI and the thickness of the layer. This technique is based on reflective interferometry. The temperature of this device does not need to be precisely controlled because RI and the layer thickness respond inversely to changes in temperature (*34*, *35*). One use of this device has been to prostate-specific antigen (PSA) by binding with PSA-antibody (*36*).

I.2.9 BioCD

The biological compact disk, or BioCD for short, uses proteins which are immobilized on a disk with a mirrored surface. This produces periodic reflective interference spectra. As molecules bind to the immobilized capture protein, the interference pattern produced is different. The extent of the binding that takes place is correlated with the difference between the interference patterns produced before and after the BioCD has been incubated with a sample (*37*, *38*). One upside of this technology is that it can be used for multiplexing when a scanner is used (*2*). A drawback of this technology is that is cannot be used for analysis of kinetics in real time.

I.2.10 Biolayer Interferometry

Biolayer interferometry (BLI) is a technique which had been commercialized by ForteBio. When white light is directed down the fiber optic, the reflected light interferes with the incoming light when it travels back up the fiber optic. The interference produces a wavelength shift that is detected by a spectrometer. In this system, capture molecules are immobilized onto the surface of a fiber optic which is then placed into a sample well. As analyte in the sample well binds to the capture molecules immobilized on the surface, the reflected interference pattern reports the change in biological layer thickness at the surface of the fiber optic. Since the signal is only measured at the surface of the fiber optic sensor, BLI can be used in extremely crude samples which are undiluted. BLI offers real-time kinetics data and is able to monitor binding specificity, association and dissociation rates with both accuracy and precision.

One major aspect of BLI is its ability to be multiplexed to run a large number of samples with a high rate of speed. BLI has been used in conjunction with 96-well and 384-well sample plates with the ability to analyze up to 96 samples in parallel (*39*, *40*). This device has been used for a variety of applications including hepatitis C detection using RNA oligonucleotides (*41*), probing protein-liposome interactions (*42*), and recognizing receptors on bone marrow dendritic cells which are bound with Pholiota nameko polysaccharides (*43*).

I.2.11 Arrayed Imaging Reflectometry

Arrayed imaging reflectometry uses destructive interference to measure binding interactions. A silicon substrate is coated with an antireflective coating. Capture molecules are also functionalized on the surface of the substrate. When no binding occurs, incident light is not reflected by the surface. When sample binds to the surface immobilized capture molecules, the destructive interference properties of the surface change and incident light is reflected. The intensity of the reflected light is proportional to the amount of the target molecule which has been captured by the surface (*23*, *44*).

Arrayed imaging reflectometry has been used in a variety of ways. This includes the development of an assay to detect and quantify influenza antibodies in human serum (*45*). Another use of this technology is for the detection of inflammatory biomarkers including cytokines in the presence of bovine serum albumin or serum (*46*).

I.2.12 Backscattering Interferometry

Every technique which has been discussed until now has required the surface immobilization of one of the molecules of interest. Surface immobilization comes at a cost which has some of the same disadvantages that a label method also has. Surface immobilization changes the nature of a molecule and could change the interaction between a surface immobilized molecule and its binding partner. Like fluorescent labels, surface immobilization require a great deal of knowledge of the molecule being immobilized. Depending

on how the molecule is immobilized and where the molecule is tethered could drastically change the interaction of the molecule with its binding partner when compared to the native interaction in a biological system (*23*, *47*).

Backscattering interferometry (BSI) is the first technique in which both surface immobilized systems as well as systems in which both proteins of interest are free in solution can be monitored. The technique was first developed using fused silica capillary tubing for small volume RI measurements (*48*). Today, BSI is now done using glass microfluidic chips requiring less than one microliter of sample to perform a measurement. Backscattering interferometry has been used to show that the level of binding observed in a surface-immobilized binding system is quite different than the same system in free-solution (*47*).

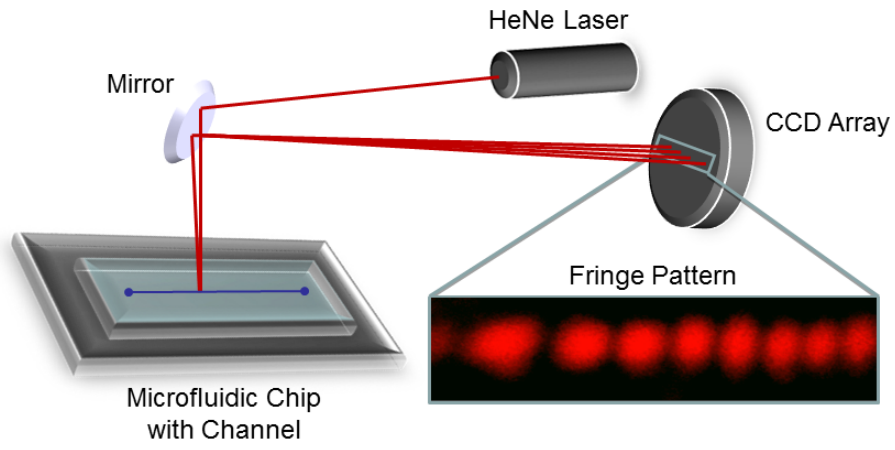

Figure I.10: Diagram of BSI setup.

The optical train to perform backscattering interferometry is quite simple (Figure I.10). Light from a HeNe laser is directed upon a fluid-filled, nearly semicircular channel at an angle that is close to normal to the plane of the chip. An interference pattern is produced

and the image of the fringe pattern is captured using a CCD linear array. As the RI of the fluid filled changes the spatial position of the interference fringes shift. The magnitude of the spatial shift is correlated to the difference in RI of the solutions that are measured. The shift has been measured using two different techniques.

One method is to measure the pixel shift of the fringes using a cross correlation method. The second method uses a fast Fourier transform to determine phase of a sample and reference interference pattern. The difference in phase between the two measurements is then found. BSI produces a series of fringes consisting of a near single-spatial frequency. By monitoring the phase of the dominant frequency in the phase of selected fringes produced by a sample and reference fluid, the phase difference can be calculated. The larger the difference in phase, the larger the difference in RI between the two fluids. As discussed earlier, binding of two proteins can change the RI of the fluid. Binding can then be correlated to the amount of change in RI (*49*, *50*).

BSI has been able to be used among a wide variety of matrixes including those which have proven difficult to work in due to potential for high background noise (*51–53*). It also has an advantage over techniques such as SPR because it is not mass dependent, meaning that BSI can measure small molecules binding to large molecules which are tethered to the sensor surface (*54*).

In its current configuration, BSI uses a single channel which means that a sample and reference are measured consecutively, not simultaneously. Therefore, temperature must be controlled throughout the experiment so that long term drift is minimized, so that variations in temperature during an experiment do not produce a false signal, signal not generated by a binding event.

I.2.13 Dual Capillary Backscattering Interferometry

One form of BSI that was developed using two capillaries to make ultrasensitive RI measurements employed simultaneous illumination of two capillaries (*13*). In this device (Figure I.11), two capillaries are mounted adjacent to one another, tilted at an angle of either +7° or -7° with respect to each other. A HeNe laser illuminates both channels at the point of intersection, with two different interference patterns being produced by each of the capillaries. The temperature of the capillaries is controlled using a Peltier thermoelectric cooler.

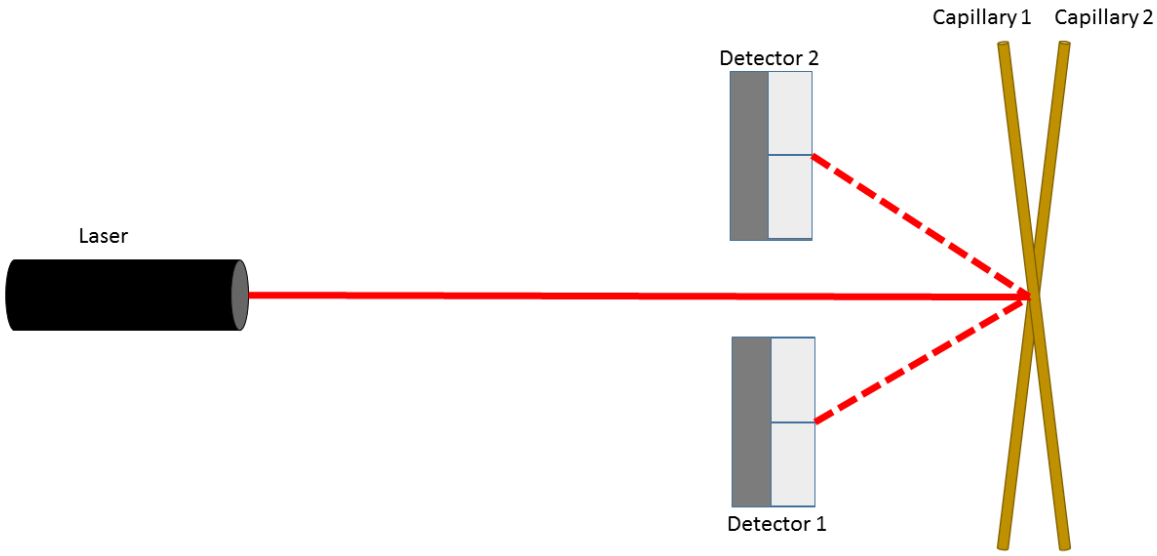

Figure I.11: Diagram of dual capillary backscattering interferometry.

Two bicell photodetectors are used to interrogate the position of a selected fringe for each interference pattern. The position of the fringe is measured based on the amount of light hitting each section of the bicell. If a fringe is aligned so that 50% of the light hits each half of the bicell, the voltage difference between the two cells is equal to zero. As the position of the fringe moves, the voltage difference is nonzero and can be correlated to the movement caused by a change in the RI of the fluid in the capillary. The algorithm to

monitor the change in voltage is as follows given that A and B are corresponding voltages from each detector.

$$Signal = \frac{A-B}{A+B} \tag{I.3}$$

Each bicell measures the signal for each capillary independently. The difference in signals between the two capillaries is then taken as the overall signal. With one capillary holding sample fluid and the other holding reference fluid, a change in temperature will cause the monitored fringe in each interference pattern to move equally. Since the two move equally, the signal change for each capillary will be equal and the difference between the two signals will be zero By using this approach, drift or false signal from temperature changes is in large part eliminated allowing detection of changes in RI as low as 10^{-9} RIU.

I.3 Conclusion

Many types of interferometry have been used to measure molecular interactions and other intrinsic properties. Their advantages include: high sensitivity, universality, and label-free operation. With the exception of BSI, all interferometers require surface immobilization which imparts complexity and cost. In the next chapter I present a new interferometric technique that is designed to provide compensation with a simple optical train.

CHAPTER II

Far Field Two Channel Interferometry

II.1 Introduction

Here a novel approach to simultaneously measuring the RI of both reference and sample fluids is reported. In far-field two channel interferometry (FF2CI), like other approaches (*6*, *8–13*) a single laser is used to illuminate two closely spaced capillaries or channels simultaneously (Figure II.1). Yet in this case, the light exiting two objects (neighboring channels or capillaries) is made to interfere. As the light exiting the objects it interferes producing a single interference pattern is produced, which reports the *difference* in optical pathlength interrogated. Since the optical train consists of two closely spaced, nearly parallel channels, it looks nominally like two slits to the incoming laser beam. Thus the outgoing fringe pattern has a predominant frequency that is fairly uniform. The phase of this single spatial frequency changes with the difference between the RIs of the media contained in adjacent channels, allowing a relative measurement to be performed. This relative measurement exhibits a significant level of compensation for temperature perturbations experienced by the fluids, thus improving performance and allowing both a sample and reference solution to be compared simultaneously.

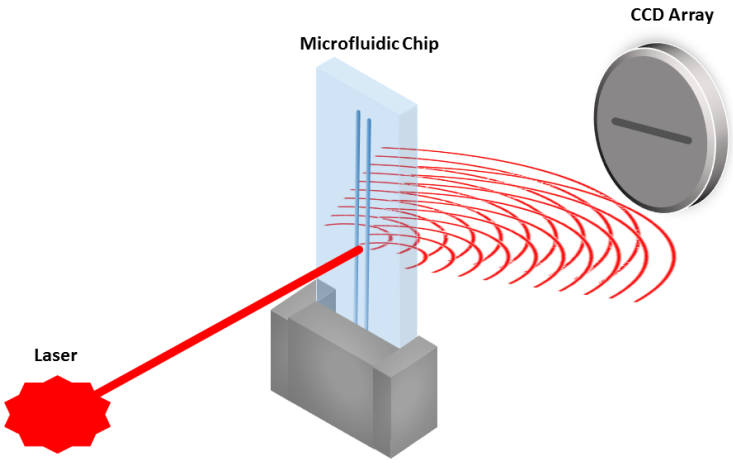

Figure II.1: Basic setup of FF2CI.

The advantages of the FF2CI approach are the intrinsic level of compensation for environmental perturbations that have an effect on RI such as temperature and source wavelength stability. In my studies I have found that the FF2CI is reasonably effective at eliminating long term drift due to environmental temperature changes. Importantly this thermal drift suppression is entirely passive and obtained without the aid of any special computer processing, as was required in dual capillary back-scattering interferometry (*13*). Because the two channels are illuminated by the same source, the FF2CI instrument also compensates for signal drift caused by instability in a laser's wavelength.

Another major advantage of the unique optical design is an interference pattern of fringes that are highly periodic and predominantly a single spatial frequency. This property enables the use of numerous position sensing approaches and algorithms, such as the fast Fourier transform (FFT) as well as signal averaging methods to improve S/N ratio for analysis. I show here that the new approach to nano-scale interferometry can be used for measurement of changes of RI in bulk fluid at a sensitivity level which enables application to chemical and biochemical assays.

II.2 Instrument Configuration

A single beam of light produced from a HeNe laser(λ=632.8 nm) was used to illuminate two closely spaced channels in a glass microfluidic chip. Light exiting each channel interfered with light from the adjacent channel creating an interference pattern (Figure II.6). The position of the interference fringes were monitored using a linear array CCD (Ames Photonics), that in turn transferred the data to a computer for analysis. All experiments were performed *without* active temperature control (Figure II.1).

II.2.1 Laser Parameters

The laser used was an unstabilized, linearly polarized, 5mW HeNe laser (25-LHP-151-249 Melles Griot) producing monochromatic light at a wavelength of 632.8 nm. The laser beam was subsequently collimated using a single-mode fiber coupler (OZ Optics) producing an homogenized, collimated beam with a spot size of 600 µm. The energy profile of the beam had a Gaussian distribution.

II.2.2 Microfluidic Chip Parameters

The glass chip (Figure II.2) used for experiments was designed and produced by Dolomite Microfluidics. The chip overall dimensions of 45 mm by 15 mm and a thickness of 4 mm. The channels were positioned 2 mm from the top surface of the chip and had dimensions of 50 µm in height and 150 µm in width. The spacing, from the centers of the channels was 230 µm resulting in a separation of 80 µm between the edges.

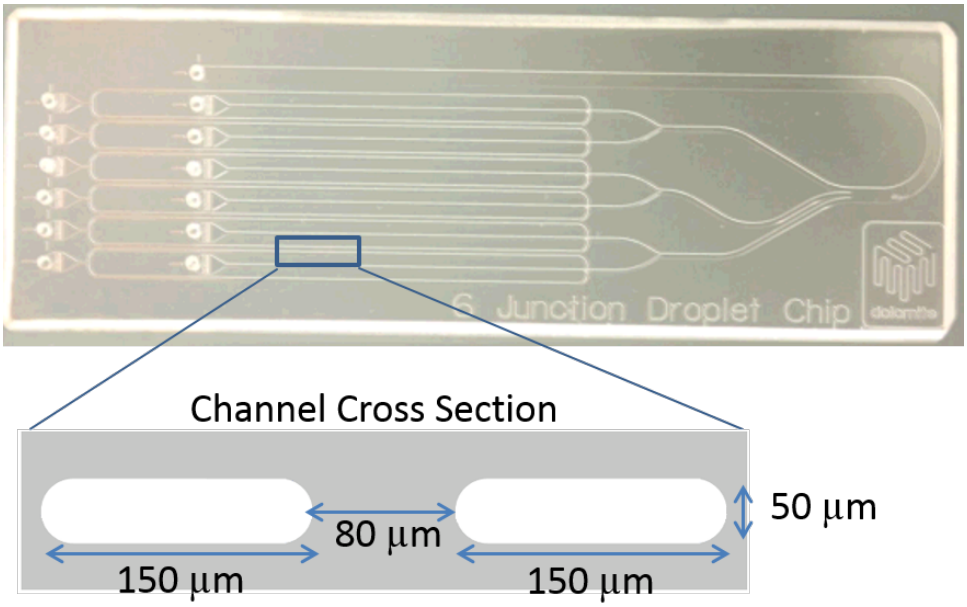

Figure II.2: Picture of microfluidic chip including diagram of channel cross-section.

The chip was attached by gluing the provided chip interface onto an aluminum block, so that the chip could be placed perpendicularly to the plane of the aluminum block. The chip was then placed inside this holder and secured with its provided connectors into the holder. In order to make small adjustments to the chip's alignment or position in both the *x* and *y* axis, the aluminum block was connected to two linear translation stages (Newport).

II.2.3 Sample Introduction

Sample fluid was introduced into each channel in the following manner. A manufacturer provided connector for the chip and a seal made from FKM fluoroelastomer was used to interface fluorinated ethylene propylene (FEP) tubing to the inlet of each channel of interest (Figure II.3). Unused channel inlets were sealed using FEP plugs.

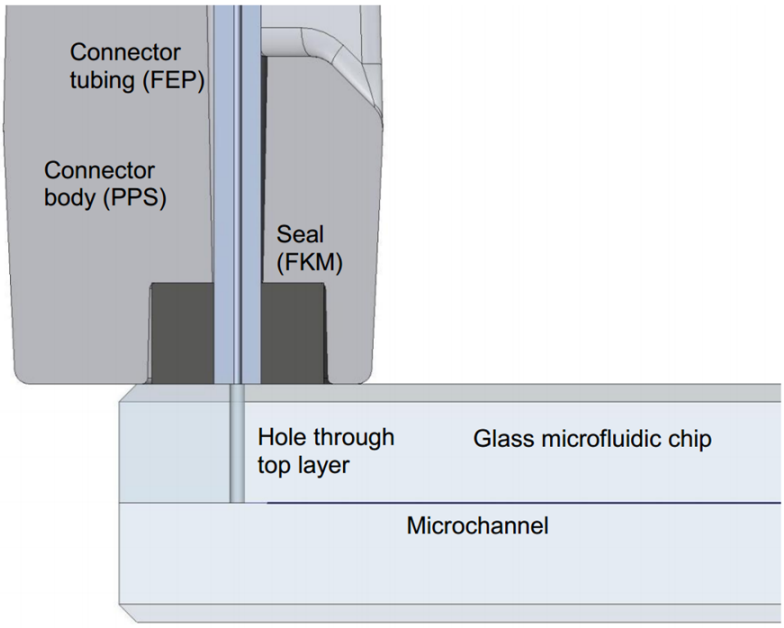

Figure II.3: Cross-section view of tubing interface with microfluidic chip (*55*).

The tubing for each channel was then attached to a port on a four port internal sample injection valve (Valco). Fill ports (Valco) allowed for a syringe to be used to introduce fluid into the separate channels (Figure II.4).

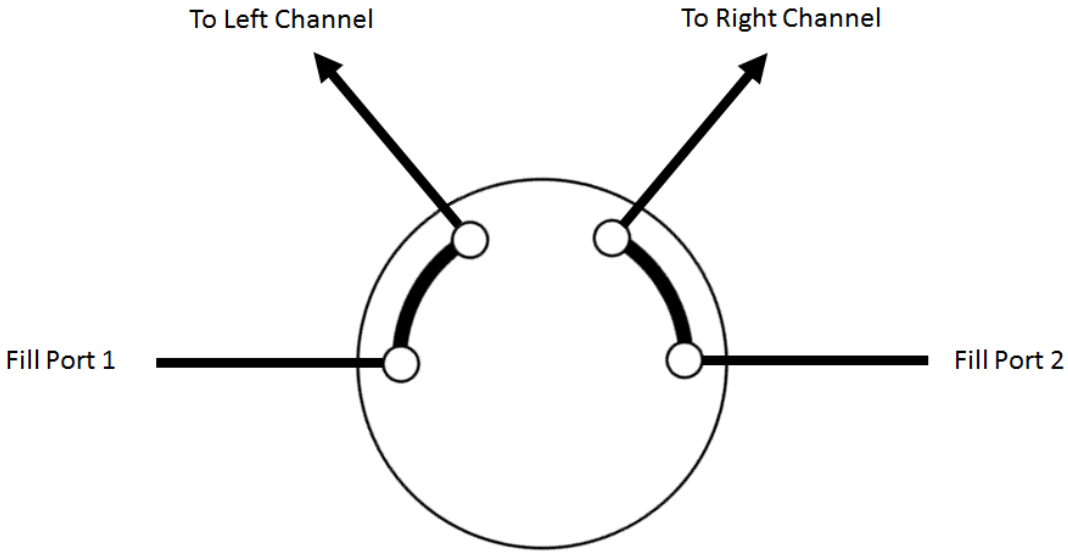

Figure II.4: Valve configuration for sample introduction.

It is important to note that the chip used in the experiments featured channels which all converged into a single channel near the end of the chip. In order to consistently make injections, it was required to inject fluid into both channels simultaneously. This procedure prevented fluid from one channel of interest from entering the other channel of interest, but made the operation of the instrument quite a bit more difficult. In future experiments it would be necessary to design a chip in which the channels of interest were completely segregated from one another and did not converge.

II.2.4 Measuring Fringe Shift

The position of the fringes is measured by using a fast Fourier transform (FFT) analysis using software written in LabView. Briefly, an integration window is selected containing a number of interference fringes (approximately ten fringes), a FFT is then performed for the selected window and a frequency vs. power spectrum in displayed (Figure II.5). Then to quantify the position of the fringes, the dominant frequency is then selected and the phase of that frequency is monitored. In Figure II.5, the top window shows the intensity per pixel of the linear CCD array. The yellow and red cursors show which series of pixels are being further analyzed in the lower window. The lower window shows the FFT frequency spectrum. As the fringes in the selected window move spatially, the phase of the dominant frequency adjusts correspondingly In Figure II.5, the top window shows the intensity per pixel of the linear CCD array. The dominant frequency is then selected using the white cursor and the phase of this frequency is monitored.

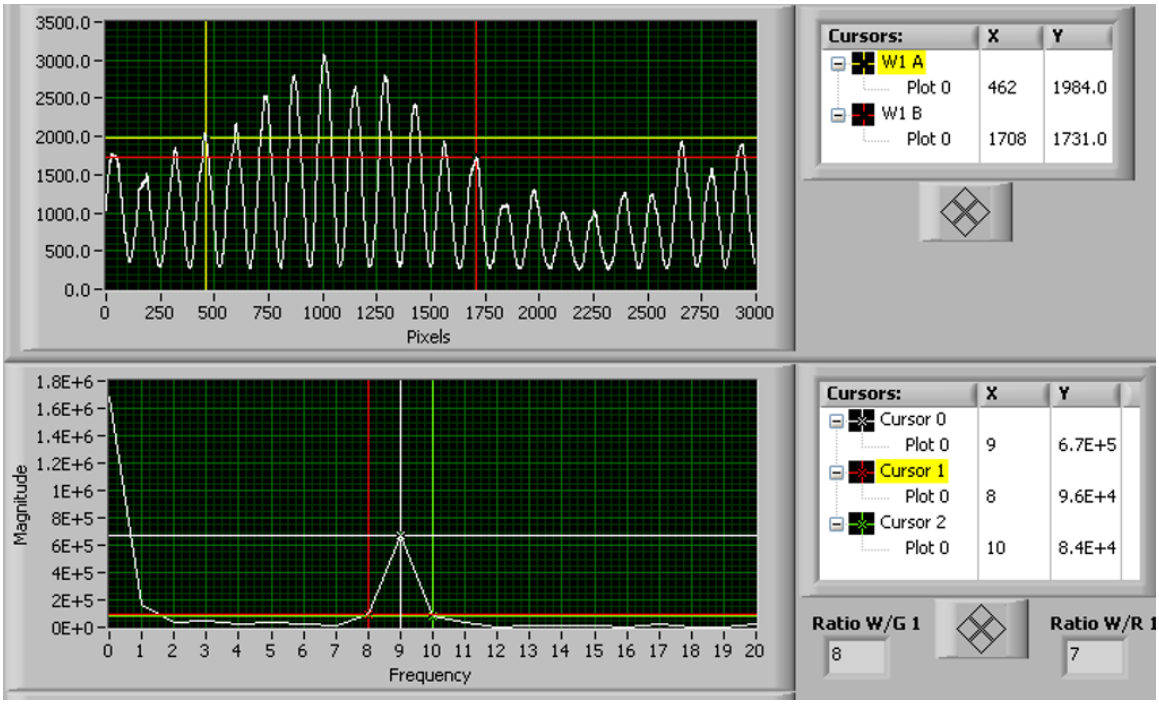

Figure II.5: Selected window and fast Fourier transform as shown in LabView data collection program.

II.3 Interference Pattern Analysis

II.3.1 Beam interference between two adjacent parallel channels

Figure II.6: Interference fringes produced in a forward scattering configuration.

A single laser is used to illuminate two separate and adjacent channels in a microfluidic chip. The channels have nearly identical dimensions (δ=1 μm). In the case described here, the channels are fluid-filled, but this interferometer can also be used to interrogate gases or moderately scattering media such as a chromatographic stationary phase. When the coherent radiation passes through each channel of nearly equal pathlength and emerges the interference patterns are made to overlap and interfere with each other. The resulting light pattern is depicted in Figure II.6.

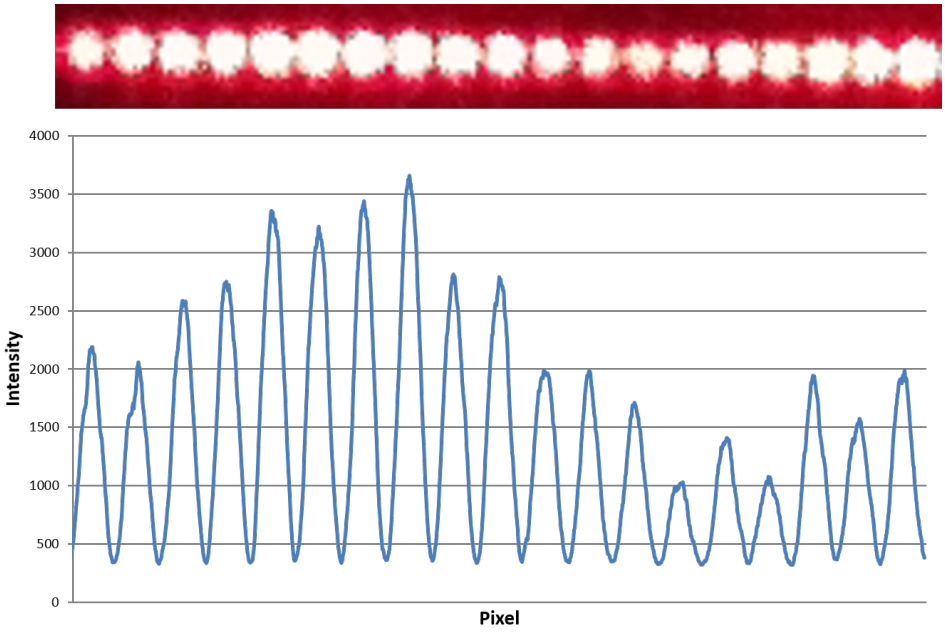

Figure II.7: Image of interference fringes and line profile of fringes collected by linear CCD array.

Figure II.7 illustrates that the fringes produced in this unique configuration have a predominant, high spatial frequency component and a lower one at about $\frac{1}{10}$ frequency. I focus on those fringes that have a nearly *single spatial frequency*. Noteworthy that these intermixed fringes have a much different energy distribution than that produced from a single channel or capillary tube (Figure II.8). Advantages of this optical train include simplicity and sample-reference comparison with environmental compensation. With reference to Figure I.3 it can be seen that the FF2CI is optically similar to a double slit experiment, and should allow me to, use the theory for this classical experiment to describe it. Thus, I will show the position of interference fringes resulting from the interaction of the two individual channels, can be predicted reasonably well using the double slit formula shown in Equation II.1.

$$d\sin\theta + (\delta_L - \delta_R) = m\lambda \tag{II.1}$$

In Equation II.1, d is equal to the distance between the centers of the two channels, θ is equal to the scattering angle, λ is the wavelength of scattered light, m is an integer, and the effective optical path length passing through the left and right channels are δ_L and δ_R respectively. The effective optical path length can be approximated using Equation II.2.

$$\delta = n * l \tag{II.2}$$

In Equation II.2, n is the RI of the fluid contained in a channel and l is the channel height. Assuming that l, the channel height, is the same for both channels, the double slit formula can be rewritten as Equation II.3.

$$d \sin\theta + (n_L - n_R)l = m\lambda \tag{II.3}$$

Using Equation II.3 and a fixed wavelength, it is possible to predict the theoretical positional shift of the interference fringes based on the difference of RI of the fluid contained in the adjacent channels.

II.3.2 Fringe Spacing Analysis

The interference pattern produced from the two channels features fringes which are very evenly spaced and feature more rapid spatial oscillations than a single channel or capillary interferometer would produce (Figure II.6). The optical configuration lends itself to being described as the classic double slit experiment, allowing the position of the fringes to be predicted by the double slit formula (Equation II.3). Using the distant screen assumption, $sin\theta = \frac{y}{D}$ in which y is the distance between the maximas of two adjacent fringes, and D is the distance from the channels to the detector screen By adjusting Equation II.3 using the distant screen assumption, it can be rewritten as Equation II.4 to determine the spacing between fringes.

$$y \approx \frac{m\lambda D}{d} \tag{II.4}$$

In this equation, y is the spacing between fringes, λ is the wavelength of the scattered light, d is the spacing between the centers of the two channels, and D is the distance from the channels to the detector. Using this equation, and the fringe pattern shown in Figure II.6 I calculated that the spacing between the centers of adjacent channels to be 223 μm. This value compares well with the expected value of 230 μm. The 7 μm discrepancy represents a percent error of 3%.

II.3.3 Neighboring channel effect on interference pattern

The interference pattern produced from illuminating two adjacent channels produces an interference pattern with a highly periodic frequency that it is profile, however it was observed that the intensity of the fringes are not uniform. It appears as though there is a low frequency carrier that is also contributing to the overall fringe pattern and I postulate that it is caused by interference from an adjacent object (channel) mixing with the two channels of interest. To test this, two interference patterns were collected. The first was produced by a laser illuminating two fluid-filled channels that were adjacent to one another. The second interference pattern was produced by illuminating a single fluid filled channel on the same chip which is parallel to the two closely spaced channels. When the resulting interference patterns are overlaid as shown in the Figure II.8, the single channel interference pattern almost traces the observed peak intensity trend observed in the two channel experiments. This observation is an unintended consequence that results from physical proximity of the channels on the chip and could be avoided, or eliminated by using a chip with only two closely spaced channels.

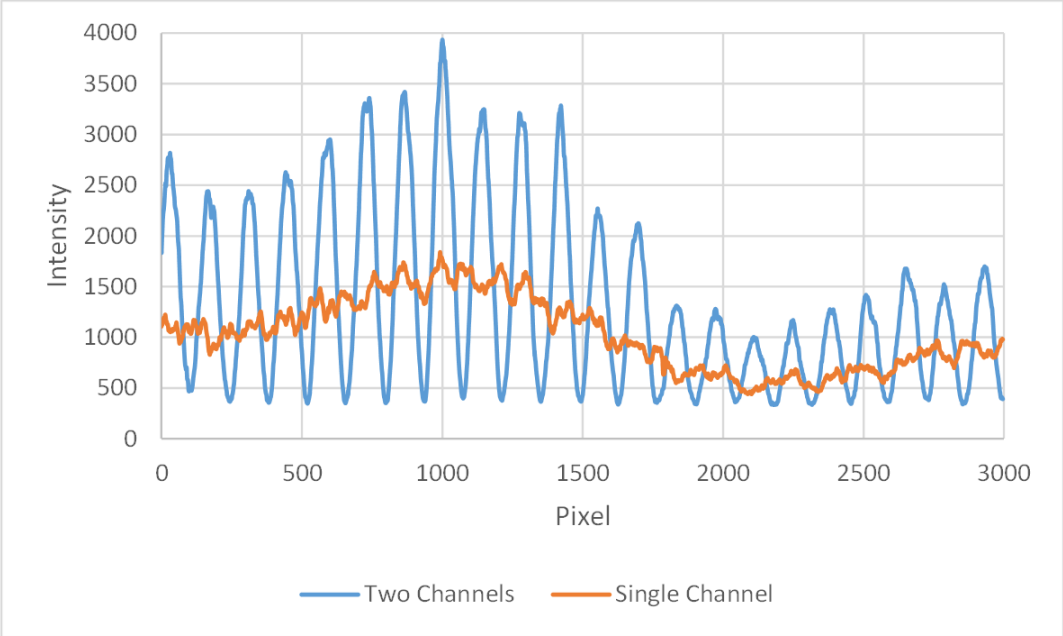

Figure II.8: Interference patterns produced by illumination of single channel (orange) and two channels (blue).

II.3.4 Sensitivity of interference patterns to a change in solution RI

Experiments were performed in both water and phosphate buffered saline (PBS). These two fluids have a significant difference in RI with phosphate buffered saline having a higher RI by $\Delta n = 2\text{x}10^{-3}$ RIU compared to water across all wavelengths (*56*). When using traditional BSI, this large of a shift in RI requires that the camera be realigned to collect the correct interference fringes. However, since this instrument is a difference measurement between two adjacent channels, the phase outputs are comparable when the fluids are matched, whether water or PBS (Figure II.9).

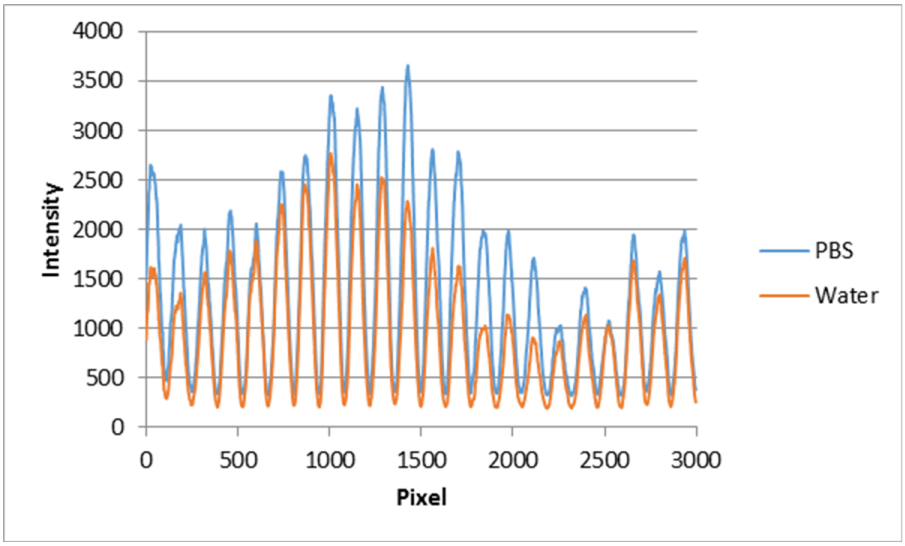

Figure II.9: Fringe pattern produced by PBS (blue) or water (orange) filled channels in selected window.

II.4 Response to changes in refractive index

As shown in Figure II.10, the device can measure the time dependent difference in RI of fluids in two parallel channels. Initially, both channels were filled with water, the instrument is balanced giving a difference in RI of zero, $\Delta n = 0$ RIU. After one minute, 20mM glycerol was injected into the ***left*** channel (Δn=2.08x10^{-4} RIU) causing a signal in the positive direction. Next, water was replaced in the left channel. This restores the signal to the baseline value as expected for a difference measurement. When a sample of 20mM glycerol was injected into the ***right*** channel ($\Delta n = -2.08$x10^{-4} RIU) the position of the fringes move resulting in a signal going in the negative direction. The observation of directionality can be explained by Equation II.3. Lastly, when 20mM glycerol was injected into the left channel ($\Delta n = 0$ RIU), matching the RI in the two channels, the signal returned to the baseline value showing that the instrument is reporting the *difference* in optical pathlength for the two channels.

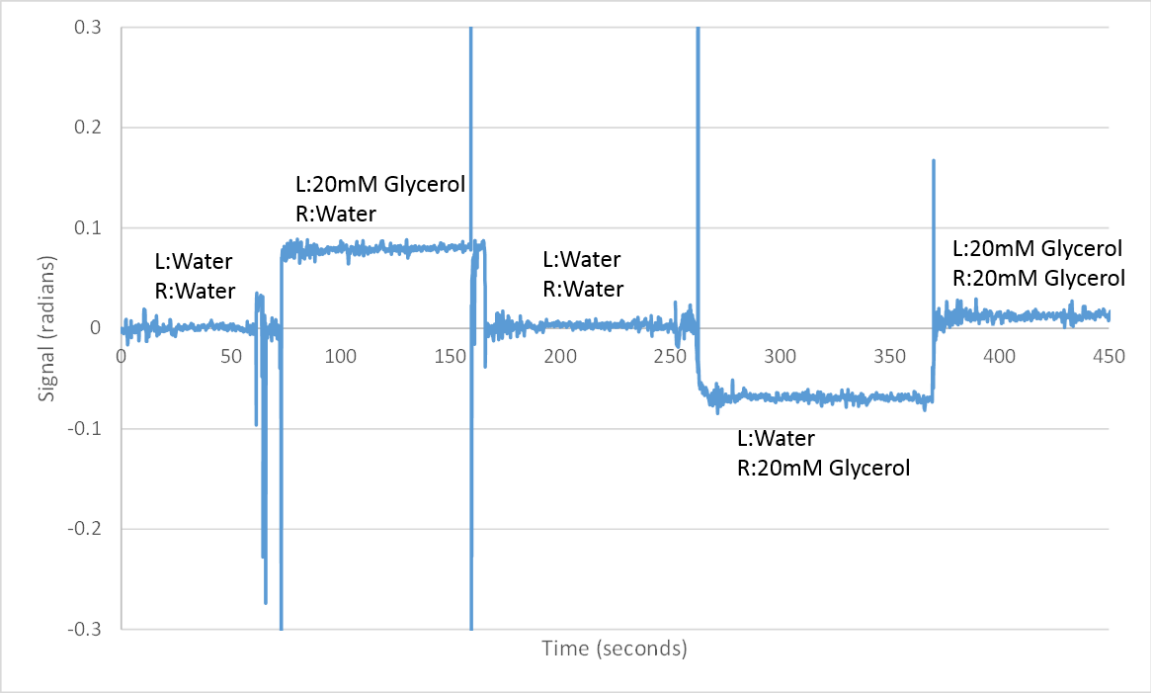

Figure II.10: Phase response to RI changes in both channels.

II.5 Analytical performance

Calibration curves were produced using glycerol solutions at concentrations of 2, 5, 10, and 20mM glycerol in either PBS or water. To determine the relative sensitivity of the channels, and thus the level of compensation possible with the instrument, sample solutions were introduced into one of the channels while the adjacent channel was filled with the appropriate reference fluid (water or PBS). This experiment was repeated for both channels. Each sample was measured from lowest to highest concentration reestablishing the baseline after each measurement to complete one trial. This was repeated until three trials had been completed (Figures II.11 and II.12).

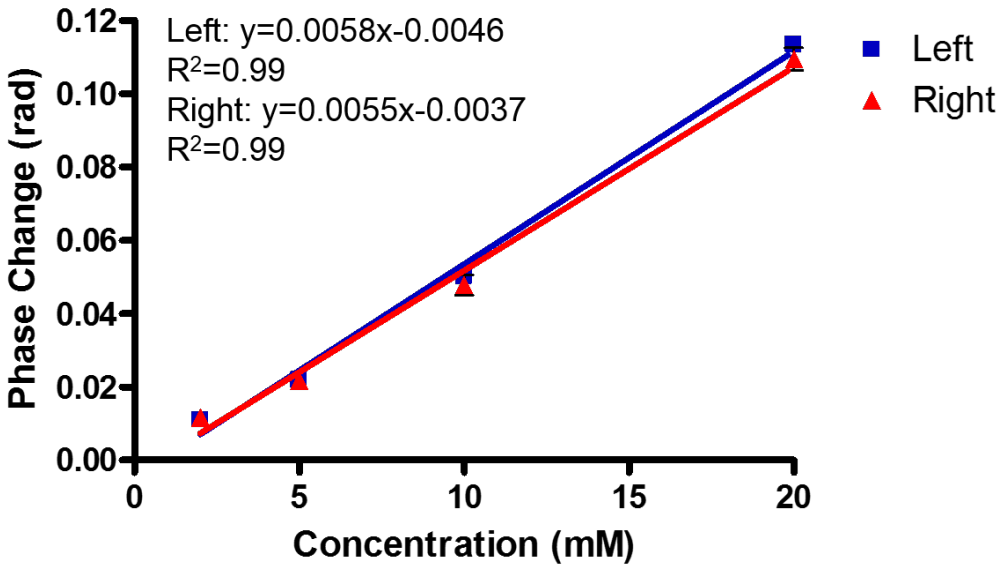

Figure II.11: Glycerol calibration in water.

For glycerol solutions in water, the sensitivity of the left channel was 558 $\frac{rad}{RIU}$ and the sensitivity of the right channel was 533 $\frac{rad}{RIU}$. The limit of detection was calculated by averaging the short term noise of all measurements taken then multiplying by three (3σ). The 3σ noise level was then divided by the slope (sensitivity) of the instrument. The LOD for the left and right channels were 1.61mM (Δn =1.67x10^{-5} RIU) and 1.65mM (Δn =1.72x10^{-5} RIU) respectively. The limit of quantification (LOQ), the reproducibility, was calculated by determining the standard deviation of replicate measurements then calculating the average. Three times this average was then divided by the slope (sensitivity) to determine the LOQ. The LOQ for the left and right channels were 1.19mM (Δn=1.24x10^{-5} RIU) and 1.26mM (Δn=1.31x10^{-5} RIU) respectively (Table II.1). Traditional BSI has a limit of quantification of approximately 0.3mM glycerol, a RI change of 3.12x10^{-6} RIU.

Table II.1: Summary of the instrument performance for water.

Channel	Limit of Detection	Limit of Quantification
Left	1.61mM (1.67x10^{-5} RIU)	1.19mM (1.24x10^{-5} RIU)
Right	1.65mM (1.72x10^{-5} RIU)	1.26mM (1.31x10^{-5} RIU)

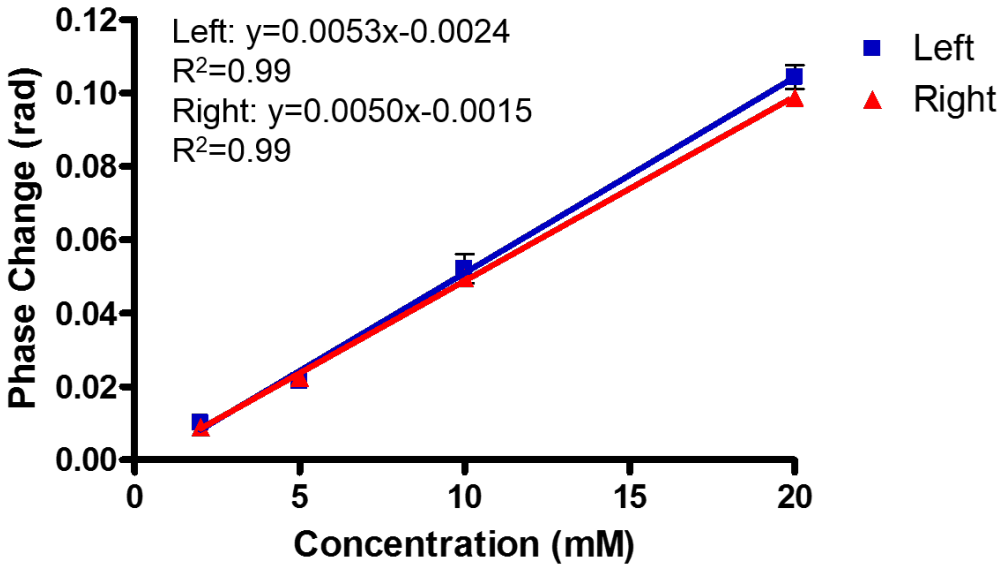

Figure II.12: Glycerol calibration in PBS.

For glycerol solutions in PBS, the sensitivity of the left channel was 512 $\frac{rad}{RIU}$ and the sensitivity of the right channel was 482 $\frac{rad}{RIU}$. The limits of detection and quantification were calculated in the same manner as previously described for water. The limits of detection for the left and right channels were 1.61mM (Δn =1.67x10^{-5} RIU) and 1.80 mM (Δn =1.87x10^{-5} RIU) respectively. The limits of quantification for the left and right channels were 1.35mM (Δn =1.40x10^{-5} RIU) and 0.79mM (Δn =8.28x10^{-6} RIU) respectively (Table II.2).

Table II.2: Summary of instrument performance for PBS.

Channel	Limit of Detection	Limit of Quantification
Left	1.61mM (1.67x10^{-5} RIU)	1.35mM (1.40x10^{-5} RIU)
Right	1.80mM (1.87x10^{-5} RIU)	0.79mM (8.28x10^{-6} RIU)

II.6 Predicting the theoretical RI sensitivity for the FF2CI

One metric for evaluating the new device is to compare the predicted path length sensitivity of a two-slit experiment to that obtained from the real chip. Here I calculate the expected performance based upon Equation II.5. As the light travels in the channels over a longer path length, there will be a larger fringe shift and thus, greater sensitivity to RI changes of the medium contained in the channel. The sensitivity can be predicted using Equation II.5 for forward scattering configurations.

$$\frac{\phi}{\Delta n} = \frac{2\pi * l}{\lambda} \tag{II.5}$$

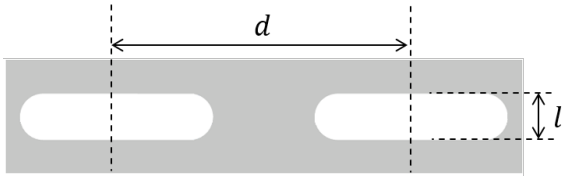

Figure II.13: Diagram of microfluidic chip showing channel separation, d, and pathlength, l.

For forward scatter configurations, as shown in Figure II.1 where the detector is collecting fringes passing the object. In this configuration the light is predicted to experience a single pass through the channels. If this is the case, the channel height, or capillary inner diameter, can be used for l in Equation II.5. Upon applying this relationship it is possible to predict the RI sensitivity of the FF2CI for a range of channel heights. The results of these calculations are presented in Figure II.14.

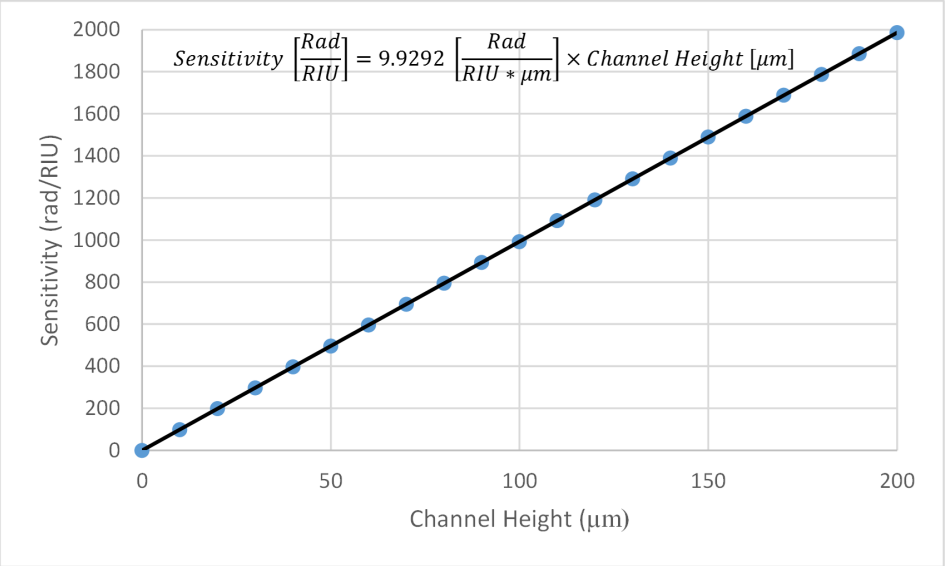

Figure II.14: Expected sensitivity based on height of channels using Equation II.5.

For our purposes, the results show that our device, with a microfluidic chip containing channels 50 µm in height, would have a predicted sensitivity of 496 $\frac{rad}{RIU}$. Simply, for every micron in channel height, the predicted RI sensitivity is about 10 radians per RIU.

II.7 Calculation of optical pathlength

For the left channel the calculated path lengths based on the calibration curves were 56.2 µm in water and 51.6 µm in PBS. For the right channel the calculated path lengths based on the calibration curves were 53.7 µm in water and 48.6 µm in PBS. The path length of the channels was calculated based on the following approximation which was given in Equation II.5. The pathlength was calculated by first finding the sensitivity ($\frac{rad}{RIU}$) for each channel, and substituting the value for $\frac{\phi}{\Delta n}$. Knowing the wavelength of the laser used, 632.8 nm, the optical pathlength, l, can be solved for. For reference, the given dimensions of the channel based on product information state that the height of the channels is 50 µm. The average pathlength for each channel using the PBS calibration data is 50.1 µm, a percent difference of 0.2% from the expected value of 50 µm.

Some work has also been done with this instrument using two fused silica capillaries instead of a microfluidic chip as a sample holder (*57*). When using the forward scattered

fringes, the expected sensitivity for each device can be closely approximated based on the dimensions of the channels or capillaries.

Table II.3: Comparison of actual and predicted sensitivity of devices.

	Capillary Device	Microfluidic Chip Device
Channel Height/ Capillary ID	250 μm	50 μm
Expected Sensitivity	2482 $\frac{rad}{RIU}$	496 $\frac{rad}{RIU}$
Actual Sensitivity	2307 $\frac{rad}{RIU}$	497 $\frac{rad}{RIU}$
Percent Difference	7%	0.2%

II.8 Difference in sensitivity between channels

In both calibration curves, the left channel displayed a higher sensitivity to RI changes than the right channel (Table II.4). In water, the left channel had a higher sensitivity by 24.8 $\frac{rad}{RIU}$. In PBS, the left channel had a higher sensitivity by 29.8 $\frac{rad}{RIU}$. The difference in sensitivity of the two channels can arise from two sources: differences in alignment and/or the physical dimensions of the two channels.

Table II.4: Difference in sensitivity between channels.

	Left Sensitivity $\frac{rad}{RIU}$	Right Sensitivity $\frac{rad}{RIU}$	Difference $\frac{rad}{RIU}$
Water	558.0	533.2	24.8
PBS	512.6	482.8	29.8

For the two channel concept to be successful to perform compensation, the two channels need to have a response function that is nearly identical. Thus when one responds to a temperature change the other must do so similarly to achieve compensation. Based on the pathlength equation, Equation II.5, a simple substitution can be made to predict the difference in response functions based on channel ***dimensions***.

$$\frac{\phi}{\Delta n} = \frac{2\pi * \Delta l}{\lambda} \tag{II.6}$$

Equation II.6 shows the difference in sensitivity between channels if their physical dimensions do not match. Δl represents the difference in channel height between two channels. If the heights of the channels differ by one micron, the two channels will differ in sensitivity by approximately 10 radians per RIU. Figure II.15 shows the calculated difference in sensitivity between channels if the channel heights are not equal.

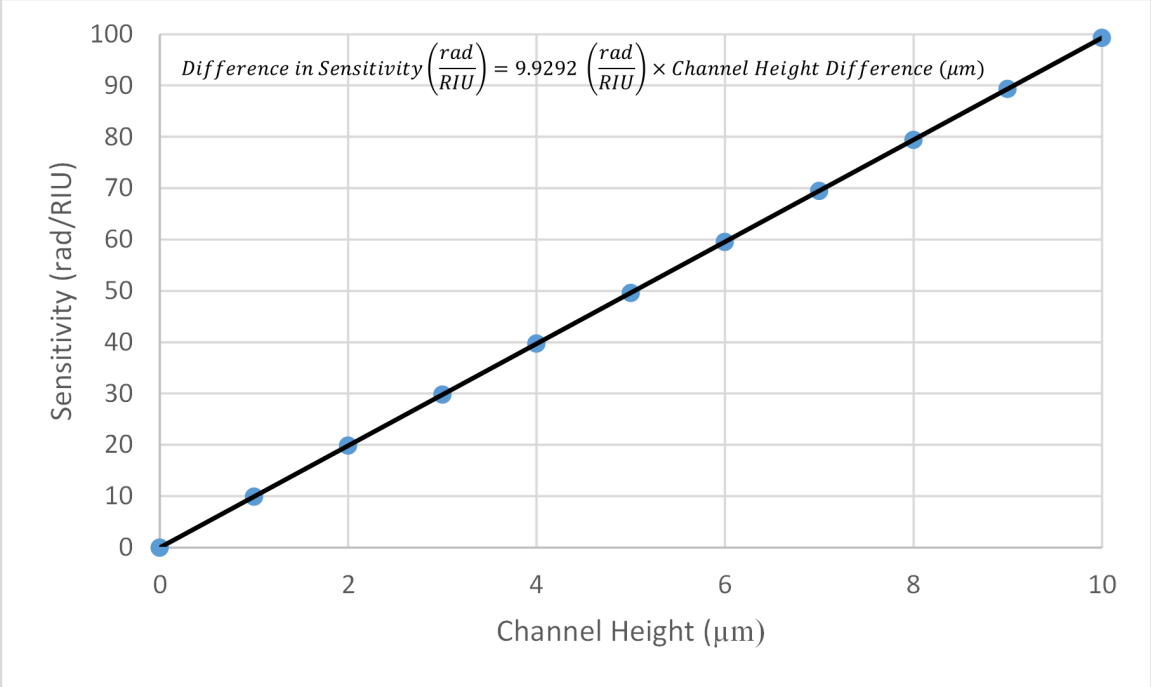

Figure II.15: Expected difference in sensitivity between channels caused by difference in channel height. Calculated using Equation II.6.

Based on chip manufacturer product information, the largest difference between the height of two channels in the chip used for these experiments is about 1 μm and the change in height along the length of a channel is 0.25 μm. Because the calculated difference in path lengths was 2.50 μm in water and 3.01 μm in PBS, I postulate that sensitivity differences between the channels is due to alignment to a greater extent than size.

II.9 Use of a low pass frequency filter to improve the LOD

One method to lower the limit of detection for a measurement is to filter the data. This is possible when the signal produced as a frequency that is discrete and separated from the noise at higher or lower frequencies. A low pass filter works by rejecting signal that has a higher frequency than a user defined threshold, allowing only signal below a certain frequency to be passed through for further analysis. By using this filter, some high frequency noise can be eliminated reducing short term noise considerably (Figure II.16) and improving the limit of detection. Figure II.16 shows the effects of filtering data. The orange trace which is unfiltered data has a higher amount of short term noise than the same data filtered shown in the blue trace.

For the glycerol curve done in PBS, a filter with a one second time constant was applied, improving the limit of detection by 33% for the left channel (1.61mM to 1.07mM). A similar level of performance improvement was realized for the right channel (34%), with the LOD dropping from 1.80mM to 1.18mM.

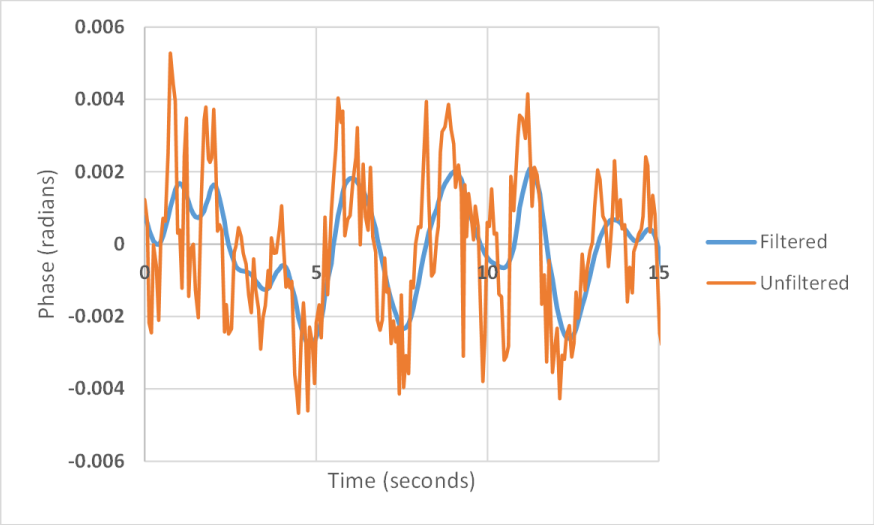

Figure II.16: Phase of filtered signal (blue) overlaid on phase of unfiltered signal (orange).

II.10 Compensation

To achieve the best compensation from sources of noise such as temperature, pressure, and wavelength changes; the left and right channels need to have nearly identical in sensitivity. If the channels do not respond equally to the same change in RI caused by the environment, namely temperature, the result will be a phase shift. The closer the sensitivity of the two channels, the more this is mitigated.

The level of compensation can be calculated by taking the difference between the slopes of the calibration curves. For the calibration curves performed, the difference was approximately 25 $\frac{rad}{RIU}$. Without temperature stabilization, the 3σ noise level is $1.7\text{x}10^{-5}$ RIU. Based on the sensitivity of each channel and the short term noise of the instrument, any change in RI to both channels that is lower than $3.6\text{x}10^{-4}$ RIU would be undetectable. The RI of water changes by approximately $1\text{x}10^{-4}\frac{RIU}{^{\circ}C}$. This means that a change in temperature of three degrees Celsius should be undetectable by the instrument.

If channels are used which have a greater channel height, each channel may exhibit greater sensitivity. To achieve the same level of compensation under the assumption that the short term noise for each system is the same, the percent difference of sensitivity between

each channel must decrease. For example, if the sensitivity of each channel increased by five times then the minimum temperature change that would be detected would decrease by five times.

II.11 Conclusion

The device is capable of measuring changes in RI to a part in 10^{-6} RIU. The sensitivity of the device could be easily improved by increasing the height of the channels which are used. Further work could be done into the possible effects of different using different channel geometry. Potential noise may even be reduced by designing a system which could actively control the temperature of the chip. With further refinement this device has the potential to be used in a variety of biochemical assays as a sample-reference configuration.

CHAPTER III

Future Work

There a number of aspects of the FF2CI which can be improved to provide better performance. In the next sections, future work that could be done in order to improve the device is discussed.

III.1 Microfluidic Chip Design

The microfluidic chip used in chapter two featured channels which converged into a single outlet. With this configuration it is possible that fluid from one channel could be pushed into the other channel which would adversely affect the measurement. If the channels were segregated with each having an independent inlet and outlet, fluid from the channels would not mix.

Some more work can be done in regards to the channel geometry used in the chip. Most importantly, the height of the channels can be adjusted which should have an impact on the sensitivity of the device to RI changes. By making the channel height larger, the device should be able to measure smaller changes in refractive index, easily reaching a level of $\Delta n = 10^{-6}$RIU and lower. By increasing the sensitivity to refractive index, the platform would have more ability to measure binding events between proteins which may not give as large of a signal which can currently be detected.

Currently, the chip in use features channels which can best be described as rectangles with rounded edges on each side. The laser currently hits the flat side of these channels. It may be interesting to see how a completely square or rectangular channel would perform as well as circular or semicircular channels.

III.2 Alignment

Currently alignment is performed using two translational stages to allow for fine movements in the x and y axis. Not to be overlooked is the angle at which the laser strikes the surface of the chip. I postulate that for the best alignment, and therefore the best sensitivity, the incoming laser needs to strike at an angle as close to normal of the surface of the chip. To allow for more precise control of the alignment it could be beneficial to place the chip on top of a stage that allows for the rotation of the chip with respect to the incoming laser beam.

It may also be beneficial to change the intensity profile of the beam. The current device uses a beam featuring a Gaussian profile. It may be easier to align the device if the beam featured a top hat profile in which a wider portion of the beam profile has a uniform intensity. If the laser beam does not interact with each channel in the same manner such as angle of incidence or intensity, then essentially two different interferometers have been produced from each channel with each having its own unique characteristics.

III.3 Potential uses of the FF2CI

The FF2CI has the potential to measure binding events between molecules which through changes in conformation, charge distribution, and hydration cause a change of the RI of the fluid that they are contained in. Dependent upon sensitivity, the devices have the potential to measure binding on a number of biological systems including protein-protein interactions, protein-antibody interactions, and protein-small molecule interactions. The device could be used for a variety of applications include K_d determination, biomarker validation, and for disease diagnosis.

BIBLIOGRAPHY

(*1*) Cooper, M. A. (2006). Optical biosensors: where next and how soon? *Drug Discovery Today 11*, 1061–1067.

(*2*) Wang, X., Zhao, M., Nolte, D. D., and Ratliff, T. L. (2011). Prostate specific antigen detection in patient sera by fluorescence-free BioCD protein array. *Biosens. Bioelectron. 26*, 1871–1875.

(*3*) Sota, H., Hasegawa, Y., and Iwakura, M. (1998). Detection of Conformational Changes in an Immobilized Protein Using Surface Plasmon Resonance. *Anal. Chem. 70*, 2019–2024.

(*4*) Elkashef, H. (1997). Laser dual-wavelength interferometric measurement of the structure and refractive parameters of carbon tetrachloride. *Opt. Mater. (Amsterdam) 8*, 175–183.

(*5*) Maroulis, G., Xenides, D., Hohm, U., and Loose, A. (2001). Dipole, dipole-quadrupole, and dipole-octopole polarizability of adamantane, C10H16, from refractive index measurements, depolarized collision-induced light scattering, conventional ab initio and density functional theory calculations. *J. Chem. Phys. 115*, 7957–7967.

(*6*) Brosinger, F., Freimuth, H., Lacher, M., Ehrfield, W., Gedig, E., Katerkamp, A., Spener, F., and Cammann, K. (1997). A label-free affinity sensor with compensation of unspecific protein interaction by a highly sensitive integrated optical Mach-Zehnder interferometer on silicon. *Sens. Actuators, B 44*, 350–355.

(*7*) Harvey, A. H., Gallagher, J. S., and Levelt Sengers, J. (1998). Revised Formulation for the Refractive Index of Water and Steam as a Function of Wavelength, Temperature and Density. *J. Phys. Chem. Ref. Data 27*, 761–774.

(*8*) Passaro, V. M. N., Dell'Olio, F., Casamassima, B., and De Leonardis, F. (2007). Guided-wave optical biosensors. *Sensors 7*, 508–536.

(*9*) Densmore, A., Vachon, M., Xu, D. X., Janz, S., Ma, R., Li, Y. H., Lopinski, G., Delage, A., Lapointe, J., Luebbert, C. C., Liu, Q. Y., Cheben, P., and Schmid, J. H. (2009). Silicon photonic wire biosensor array for multiplexed real-time and label-free molecular detection. *Opt. Lett. 34*, 3598–3600.

(*10*) Ymeti, A., Kanger, J. S., Greve, J., Lambeck, P. V., Wijn, R., and Heideman, R. G. (2003). Realization of a multichannel integrated Young interferometer chemical sensor. *Appl. Opt. 42*, 5649–5660.

(*11*) Wang, J., Xu, X., Zhang, Z., Yang, F., and Yang, X. (2009). Real-Time Study of Genomic DNA Structural Changes upon Interaction with Small Molecules Using Dual-Polarization Interferometry. *Anal. Chem. 81*, 4914–4921.

(*12*) Wang, J., Coffey, P. D., Swann, M. J., Yang, F., Lu, J. R., and Yang, X. (2010). Optical Extinction Combined with Phase Measurements for Probing DNA-Small-Molecule Interactions Using an Evanescent Waveguide Biosensor. *Anal. Chem. 82*, 5455–5462.

(*13*) Wang, Z., and Bornhop, D. J. (2005). Dual-Capillary Backscatter Interferometry for High-Sensitivity Nanoliter-Volume Refractive Index Detection with Density Gradient Compensation. *Anal. Chem. 77*, 7872–7877.

(*14*) Yuan, J., Zhao, C., Ye, M., Kang, J., Zhang, Z., and Jin, S. (2014). A Fresnel reflection-based optical fiber sensor system for remote refractive index measurement using an OTDR. *Photonic Sensors 4*, 48–52.

(*15*) Christie, W., *Detectors for HPLC of lipids with special reference to evaporative light-scattering detection*; Oily Press: 1992.

(*16*) Herschel, W. (1805) *Philos. Trans. R. Soc. 95*, 31–64.

(*17*) Baldwin, J., and Haniff, C. (2002). The application of interferometry to optical astronomical imaging. *Philos. Trans.:Math., Phys. Eng. Sci. 360*, 969–986.

(*18*) van Deelen, W., and Nisenson, P. (1969). Mirror blank testing by real-time holographic interferometry. *Appl Opt 8*, 951–5.

(*19*) Bruning, J. H., Herriott, D. R., Gallagher, J. E., Rosenfeld, D. P., White, A. D., and Brangaccio, D. J. (1974). Digital wavefront measuring interferometer for testing optical surfaces and lenses. *Appl Opt 13*, 2693–703.

(*20*) Scudieri, F. (1980). Differential interferometric method for optical fiber testing. *Appl Opt 19*, 404–408.

(*21*) Massonnet, D, Rossi, M, Carmona, C, Adragna, F, Peltzer, G, Feigl, K, and Rabute, T (1993) *Nature 364*, 138–142.

(*22*) Vincent, P., Larsen, S., Galloway, D., Laczniak, R., Walter, W., Foxall, W., and Zucca, J. (2003) *Geophys. Res. Lett. 30*, 2141–5.

(*23*) Kussrow, A., Enders, C. S., and Bornhop, D. J. (2012). Interferometric Methods for Label-Free Molecular Interaction Studies. *Anal. Chem. 84*, 779–792.

(*24*) Schneider, B. H., Dickinson, E. L., Vach, M. D., Hoijer, J. V., and Howard, L. V. (2000). Optical chip immunoassay for hCG in human whole blood. *Biosens. Bioelectron. 15*, 597–604.

(*25*) Goh, J. B., Loo, R. W., and Goh, M. C. (2005). Label-free monitoring of multiple biomolecular binding interactions in real-time with diffraction-based sensing. *Sens. Actuators, B 106*, 243–248.

(*26*) Barrios, C. A., Zhenhe, C., Navarro-Villoslada, F., Lopez-Romero, D., and Moreno-Bondi, M. C. (2011). Molecularly imprinted polymer diffraction grating as label-free optical bio(mimetic)sensor. *Biosens. Bioelectron. 26*, 2801–2804.

(*27*) Cleverley, S., Chen, I., and Houle, J.-F. (2010). Label-free and amplified quantitation of proteins in complex mixtures using diffractive optics technology. *J. Chromatogr. B: Anal. Technol. Biomed. Life Sci. 878*, 264–270.

(*28*) Lee, T.-H., Hall, K. N., Swann, M. J., Popplewell, J. F., Unabia, S., Park, Y., Hahm, K.-S., and Aguilar, M.-I. (2010). The membrane insertion of helical antimicrobial peptides from the N-terminus of Helicobacter pylori ribosomal protein L1. *Biochim. Biophys. Acta, Biomembr. 1798*, 544–557.

(*29*) Qavi, A. J., Washburn, A. L., Byeon, J.-Y., and Bailey, R. C. (2009). Label-free technologies for quantitative multiparameter biological analysis. *Anal. Bioanal. Chem. 394*, 121–135.

(*30*) Vollmer, F., and Arnold, S. (2008). Whispering-gallery-mode biosensing: label-free detection down to single molecules. *Nat. Methods 5*, 591–596.

(*31*) Armani, A. M., Kulkarni, R. P., Fraser, S. E., Flagan, R. C., and Vahala, K. J. (2007). Label-Free, Single-Molecule Detection with Optical Microcavities. *Science 317*, 783–787.

(*32*) Nikitin, P. I., Grigorenko, A. N., Beloglazov, A. A., Valeiko, M. V., Savchuk, A. I., Savchuk, O. A., Steiner, G., Kuhne, C., Huebner, A., and Salzer, R. (2000). Surface plasmon resonance interferometry for micro-array biosensing. *Sens. Actuators, A 85*, 189–193.

(*33*) Wu, C.-M., Jian, Z.-C., Joe, S.-F., and Chang, L.-B. (2003). High-sensitivity sensor based on surface plasmon resonance and heterodyne interferometry. *Sens. Actuators, B 92*, 133–136.

(*34*) Proll, G., Markovic, G., Steinle, L., and Gauglitz, G. (2009). Reflectometric interference spectroscopy. *Methods Mol. Biol. (Totowa, NJ, U. S.) 503*, 167–178.

(*35*) Gauglitz, G. (2005). Direct optical sensors: principles and selected applications. *Anal. Bioanal. Chem. 381*, 141–155.

(*36*) Choi, J.-M., An, J.-Y., and Kim, B.-W. (2009). Effect of biolinker on the detection of prostate specific antigen in an interferometry. *Biotechnol. Bioprocess Eng. 14*, 6–12.

(*37*) Varma, M. M., Nolte, D. D., Inerowicz, H. D., and Regnier, F. E. (2004). Spinning-disk self-referencing interferometry of antigen-antibody recognition. *Opt Lett 29*, 950–2.

(*38*) Varma, M. M., Inerowicz, H. D., Regnier, F. E., and Nolte, D. D. (2004). High-speed label-free detection by spinning-disk micro-interferometry. *Biosens. Bioelectron. 19*, 1371–1376.

(*39*) fortebio.com.

(*40*) Do, T., Ho, F., Heidecker, B., Witte, K., Chang, L., and Lerner, L. (2008). A rapid method for determining dynamic binding capacity of resins for the purification of proteins. *Protein Expression Purif. 60*, 147–150.

(*41*) Roh, C., Kim, S.-E., and Jo, S.-K. A simple and rapid detection of viral protein using RNA oligonucleotide in a biosensor.

(*42*) Wallner, J., Lhota, G., Jeschek, D., Mader, A., and Vorauer-Uhl, K. (2013). Application of Bio-Layer Interferometry for the analysis of protein/liposome interactions. *J. Pharm. Biomed. Anal. 72*, 150–154.

(*43*) Li, H., Tao, Y., Zhao, P., Ban, X., Zhi, D., Li, G., Wang, F., Yang, X., and Huai, L. Recognition of receptors on bone marrow-derived dendritic cells bound with Pholiata nameko polysaccharides., 2015.

(*44*) Mace, C. R., Striemer, C. C., and Miller, B. L. (2006). Theoretical and Experimental Analysis of Arrayed Imaging Reflectometry as a Sensitive Proteomics Technique. *Anal. Chem. 78*, 5578–5583.

(*45*) Mace, C. R., Topham, D. J., Mosmann, T. R., Quataert, S. A., Treanor, J. J., and Miller, B. L. (2011). Label-free, arrayed sensing of immune response to influenza antigens. *Talanta 83*, 1000–5.

(*46*) Carter, J. A., Mehta, S. D., Mungillo, M. V., Striemer, C. C., and Miller, B. L. (2011). Analysis of inflammatory biomarkers by Arrayed Imaging Reflectometry. *Biosens. Bioelectron. 26*, 3944–3948.

(*47*) Pesciotta, E. N., Bornhop, D. J., and Flowers, R. A., II (2011). Back-scattering interferometry: a versatile platform for the study of free-solution versus surface-immobilized hybridization. *Chem. - Asian J. 6*, 70–73.

(*48*) Bornhop, D. J. (1995). Microvolume index of refraction determinations by interferometric backscatter. *Appl Opt 34*, 3234–9.

(*49*) Markov, D. A., Swinney, K., and Bornhop, D. J. (2004). Label-Free Molecular Interaction Determinations with Nanoscale Interferometry. *J. Am. Chem. Soc. 126*, 16659–16664.

(*50*) Markov, D., Begari, D., and Bornhop, D. J. (2002). Breaking the 10-7 barrier for RI measurements in nanoliter volumes. *Anal. Chem. 74*, 5438–5441.

(*51*) Baksh, M. M., Kussrow, A. K., Mileni, M., Finn, M. G., and Bornhop, D. J. (2011). Label-free quantification of membrane-ligand interactions using backscattering interferometry. *Nat. Biotechnol. 29*, 357–360.

(*52*) Bornhop, D. J., Latham, J. C., Kussrow, A., Markov, D. A., Jones, R. D., and Sorensen, H. S. (2007). Free-Solution, Label-Free Molecular Interactions Studied by Back-Scattering Interferometry. *Science 317*, 1732–1736.

(*53*) Kussrow, A., Enders, C. S., Castro, A. R., Cox, D. L., Ballard, R. C., and Bornhop, D. J. (2010). The potential of backscattering interferometry as an in vitro clinical diagnostic tool for the serological diagnosis of infectious disease. *Analyst 135*, 1535–1537.

(*54*) Kussrow, A., Kaltgrad, E., Wolfenden, M. L., Cloninger, M. J., Finn, M. G., and Bornhop, D. J. (2009). Measurement of Monovalent and Polyvalent Carbohydrate-Lectin Binding by Back-Scattering Interferometry. *Anal. Chem. (Washington, DC, U. S.) 81*, 4889–4897.

(*55*) dolomite-microfluidics.com.

(*56*) Zhernovaya, O., Sydoruk, O., Tuchin, V., and Douplik, A. (2011). The refractive index of hemoglobin in the visible range. *Phys. Med. Biol. 56*, 4013–4021.

(*57*) Bieske, E. J. (2014). Double capillary interferometer for sensitive refractive index measurements of fluids. *Manuscript In Preparation*.